Journal of New Materials for Electrochemical Systems 15, 129-135 (2012)

Electrochemical Properties of Nanostructured Ag_xPt_{100-x}/C Electrocatalyst for Oxygen Reduction Reaction

Andrés Godínez-García[*,1], Alejandra García-García[2,5], H. Vladimir Martínez-Tejada[3], J.F. Pérez-Robles[1] and O. Solorza-Feria[4]

[1]Depto. Materiales, CINVESTAV-IPN, Libramiento Norponiente 2000 Fracc. Real de Juriquilla, C.P. 76230 Querétaro, Qro., México
[2] Centro de Investigación en Materiales Avanzados S.C. Unidad Monterrey,
Alianza Norte #202 Km10 de la Autopista Monterrey-Aeropuerto. C.P. 66600, Apodaca, Nuevo León, México
[3]Grupo de Energía y Termodinámica, Universidad Pontificia Bolivariana, Medellín, Antioquia, C.P. 050031, Colombia
[4]Depto. Química, CINVESTAV-IPN, Av. IPN 2508 A.P. 14-740, 07360 México, D.F., México
[5]University of Texas at San Antonio, Dpt. Physics and Astronomy, One UTSA circle, 78249. San Antonio, TX. USA

Received: December 10, 2011, Accepted: February 10, 2012, Available online: April 03, 2012

Abstract: *In this work, Ag_xPt_{100-x}/C (x = 60, 80, 90 and 95) colloidal nanostructured electrocatalysts for the oxygen reduction reaction (ORR) were prepared by sequential reduction of $AgNO_3$ and H_2PtCl_6 using an ultrasound-assisted colloidal method. The synthesized materials were characterized by UV/Vis spectroscopy, XRD, EDS and HRTEM. In addition electrochemical measurements were performed using cyclic voltammetry (CV) and thin-film rotating-disk electrode (TF-RDE) technique in 0.5 M H_2SO_4 at room temperature. Results of the physical characterization showed ring-like morphology of the nanostructured catalyst with a size distribution in the range of 6-16 nm. From steady polarization measurements, the Ag_xPt_{100-x}/C nanocatalysts showed electrocatalytic activity towards the ORR like that obtained for Pt/C catalyst under the same experimental conditions and also favored the multielectron ($n=4e^-$) charge transfer process to water formation (i.e., $O_2+4H^++4e^-\rightarrow 2H_2O$).*

Keywords: Nanoparticles, Sonochemistry, Electrochemical properties, ORR, PEMFC

1. INTRODUCTION

Proton exchange membrane PEM fuel cells are electrochemical devices that will play a fundamental role in the new hydrogen technologies due to their ability to substitute combustion engines in automobiles [1, 2]. Nevertheless, before this becomes a reality, some issues must be solved, related to the availability of stable materials with reduced cost for electroctalysts and membranes that allow a low-cost and a mass production of PEM fuel cells [3]. For the future energy economy supported by hydrogen, although platinum is the best catalyst used to enhance the kinetic of the hydrogen oxidation and oxygen reduction reaction (ORR) that take place in a PEMFC**,** is not fully adequate due to its high cost and relative scarcity. Additionally, the high performance of fuel cells (FCs) is usually reported using pure hydrogen as a fuel. However, from the technological point of view this is not a realistic alternative for now, since most of the hydrogen is obtained from reformation of natural gas so that it contains traces of CO, which are strongly adsorbed on the surface of Pt, poisoning active sites for the hydrogen catalytic dissociation reaction [4]. In this sense, one of the main technical problems lies in the partial or complete substitution of platinum as electrocatalyst for PEM fuel cells.

For several years, different research groups around the world have been looking for alternative materials or reduce the amount of platinum required for a good performance of FCs [5-7]. There are different strategies to reduce the amount of platinum and to reach the target of the U.S. Department of Energy (DOE) for the cost of fuel cell system that will be $30/kW in 2015 [8]. One of these strategies is to develop nanostructures with core-shell morphology. The core-shell morphology consists of one type of atom surrounding a core of another type of atom**.** This kind of nanos-

*To whom correspondence should be addressed: Email: agodinez@qro.cinvestav.mx
Phone:

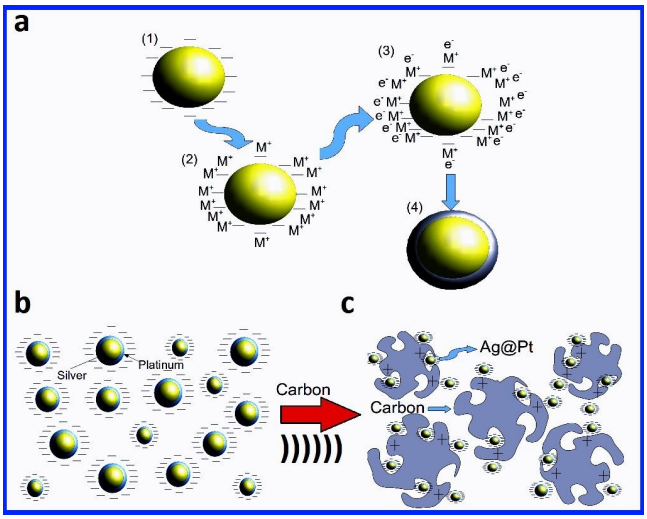

Figure 1. Schematic of the core-shell synthesis of nanoparticles, Ag@Pt, using an ultrasound-assisted colloidal method: (a) shell formation, (b) colloidal suspension and (c) supported nanoparticles on carbon black.

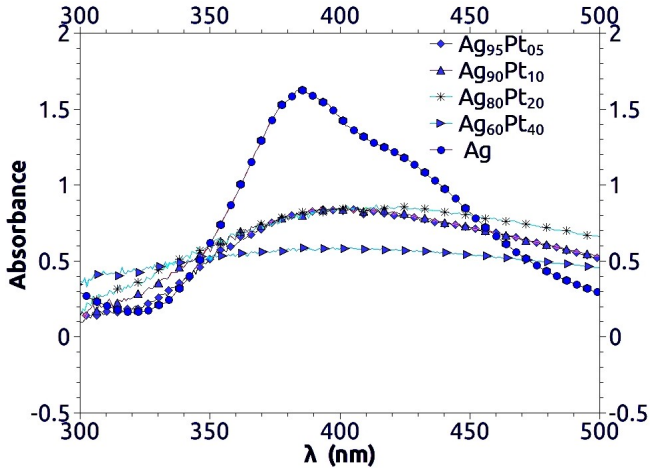

Figure 2. UV/Vis spectra of silver-platinum nanoparticles whose approximate composition is $Ag_{95}Pt_{05}$, $Ag_{90}Pt_{10}$, $Ag_{80}Pt_{20}$ and $Ag_{60}Pt_{40}$, all trisodium citrate stabilized.

tructures can help to decrease the amount of platinum in fuel cells, and therefore their cost [9]. However, these structures can be modified by galvanic substitution caused by the reactive precursors, as it has been observed in some core-shell systems [10]. If the morphology of the core-shell is modified, the electroactivity of the material is changed affecting the activity for the ORR. Thus, to study the catalytic activity of structures modified by galvanic substitution represents an important goal.

In this work nanostructures of Ag_xPt_{100-x} supported in carbon black were studied. This system is known that presents galvanic substitution [11]. In order to synthesize such nanostructures a procedure using sodium citrate as surface modifier for obtaining core-shell nanoparticles was followed, as reported in previous studies [12-15]. The nanostructures in solution were supported in carbon black, previously treated by HNO_3[16]. Sonochemistry has quickly become a very important technique in the synthesis of nanostructured materials; because of the improved properties that high intensity ultrasound induces on nanomaterials, such as cleaner surface and excellent dispersion on different supports. [17] In this case it is used to obtain well-dispersed nanoparticles in carbon black.

The nanostrured materials were characterized by UV/Vis spectroscopy; XRD, EDX and HRTEM, showing a ring-like morphology. The kinetic parameters of the ORR on carbon-supported materials were measured in order to elucidate the activity of the oxygen reduction reaction using a thin film rotating disk electrode (TF-RDE). These last results contribute to compare the catalytic activity for the ORR of the bimetallic catalyst to polycrystalline platinum.

2. EXPERIMENTAL PROCEDURE

2.1. Synthesis

The synthesis of core-shell nanoparticles was carried out using hexachloroplatinic acid ($H_2PtCl_6 \cdot 6H_2O$) and silver nitrate ($AgNO_3$) as precursors of Pt and Ag, respectively. Trisodium citrate dehydrated as the surface modifier.

Colloidal silver solutions were prepared using 4.63, 4.39, 3.9 and 2.93 mM concentrations of $AgNO_3$ aqueous solutions. Then 1.02 mM of trisodium citrate was added to each solution. The silver ions were reduced by 1.51 mM of sodium borohydride ($NaBH_4$), which was in excess to reduce also the platinum ions to form the platinum shell.

To form the shell, the colloidal silver solutions were subjected to high-intensity sonication (Sonics and Materials Ultrasonic Processor®, standard probe, 0.5 in, 100 W/cm^2), while 50 ml of aqueous solution of H_2PtCl_6, at 0.975, 1.95, 3.90 and 7.80 mM was added to each solution, yielding approximately $Ag_{95}Pt_{05}$, $Ag_{90}Pt_{10}$, $Ag_{60}Pt_{40}$ and $Ag_{80}Pt_{20}$ as estimated compositions.

Solutions of colloidal core-shell particles were dispersed into 300mg Vulcan XC-72 (Cabot®) porous carbon, which was added while the solution was under ultrasonic vibration. The porous carbon was previously subjected to a cleaning and functionalization process with HNO_3 to remove impurities and to create positive acidic sites. The carbon attracted the core-shell colloidal particles, which leads to the precipitation as powder. The precipitate was washed several times with deionized water and dried. This procedure yielded the Ag_xPt_{100-x}/C electrocatalysts, which were subsequently characterized. In order to compare the catalytic activity of the obtained electrocatalysts a commercial 20wt.% Pt/C-Etek catalyst was used as a comparative reference.

2.2. Characterization

The size of the Ag_xPt_{100-x} nanoparticles and the morphology of the Ag_xPt_{100-x}/C composites were characterized by high-resolution transmission electron microscopy (HRTME) using a JEM-2010F FEG-TEM equipment, operated at 200kV. To obtain the diffraction pattern, a fast Fourier transform (FFT) was applied, using Digital Micrograph software. A Rigaku X-ray diffractometer (XRD) with Co Ka radiation (λ= 1.78899 Å), operated at 30 kV and 16 mA, was employed to determine the phases present in the catalysts, as well as their crystallite sizes. Energy dispersive X-ray spectrometry (EDX), using a Philips XL-30 environmental scanning electron

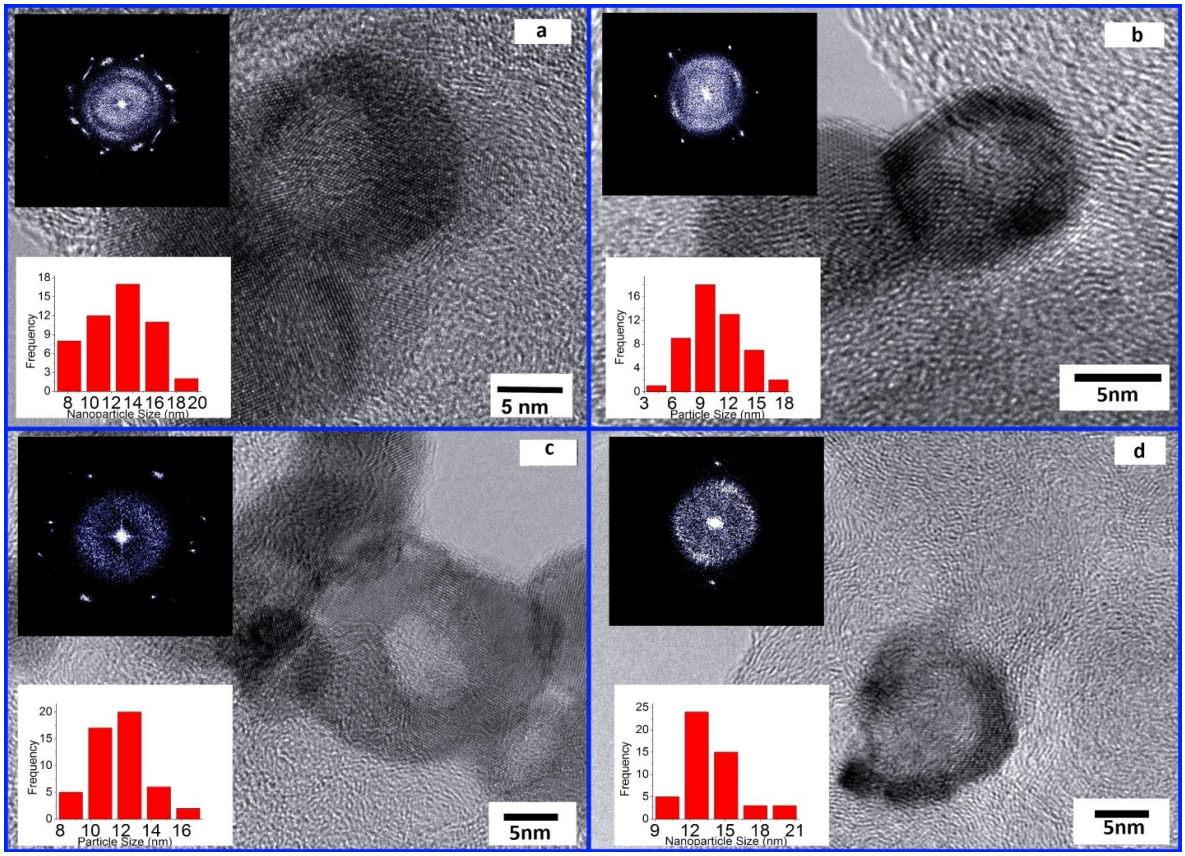

Figure 3. HRTEM micrographs for Ag_xPt_{100-x}: (a) $Ag_{95}Pt_{05}$/C, (b) $Ag_{90}Pt_{10}$/C, (c) $Ag_{80}Pt_{20}$/C and (d) $Ag_{60}Pt_{40}$/C. The upper-left side of each image is the diffraction pattern of the darker region for each particle and the lower-left side is the particle size distribution.

microscope (ESEM), was used to determine the chemical composition of the nanoparticles.

The catalytic activity was determined by cyclic voltammetry (CV), using a three-electrode test cell at room temperature. A thin-film electrode technique was used to obtain the voltammetric curves. A 5 mm diameter glassy carbon disk held in a Teflon cylinder was used as the working electrode, on which a thin-layer of Nafion-impregnated catalyst was cast. The loading of both catalysts, Ag_xPt_{100-x}/C and Pt/C, on the electrode was 0.64mg/cm^2. A platinum mesh was used as the counter electrode and Hg/Hg_2SO_4/0.5M H_2SO_4 (MSE = 0.680 V/NHE) as the reference electrode. The potentials in the electrochemical experiments were referred to NHE (normal hydrogen electrode). Electrochemical studies were performed with a Voltalab PGZ402 potentiostat. The electrolyte was a 0.5M H_2SO_4 solution, prepared from deionized water, which was degassed with ultrahigh-purity N_2. The electrolytic solution was saturated using O_2 in order to study the oxygen reduction reaction.

3. RESULTS AND DISCUSSION

The ultrasound-assisted colloidal process started with the formation of charged silver nanoparticles, which were stabilized by a surface modifier (trisodium citrate) [13]. The negatively charged particles of silver, attract the positive ions of the other metal, forming in this way a shell of ions, which later were reduced to zero-valent metal, M^0, by the reducing agent ($NaBH_4$). These colloidal particles were formed with an excess of negative charge and were adsorbed onto the surface of high porosity carbon, taking advantage of its positively charged cavities. The positive charges of the carbon were generated by an acid treatment using HNO_3 [16]. The ultrasonic pretreatment destroys the agglomerated carbon particles, increasing both the available area for adsorption of the colloidal particles and the reactive area [17]. A scheme of the synthesis process is depicted in Fig. 1.

Fig. 1a shows the formation of the platinum shell on silver, which consists of four stages: (1) formation of colloidal silver, (2) attraction of Pt^{4+} positive ions to the surface of Ag nanoparticles, (3) reduction of Pt^{4+} ions by $NaBH_4$ to Pt^0, and (4) union of Pt atoms on the surface of Ag. Then the nanoparticles were kept in suspension by electrostatic forces generated by the negative citrate groups (Fig. 1b) [13]. The same negative charges favored the surface adsorption of functionalized carbon by acid groups produced by the HNO_3 (Fig. 1c) [16].

The first characterization to elucidate the interaction between silver and platinum was carried out by UV/Vis spectroscopy [12]. Fig. 2 shows the plasmon absorption spectra of the colloidal suspensions of all the samples; it is noted that when platinum precursor is added, the absorption spectrum differ from that of alone col-

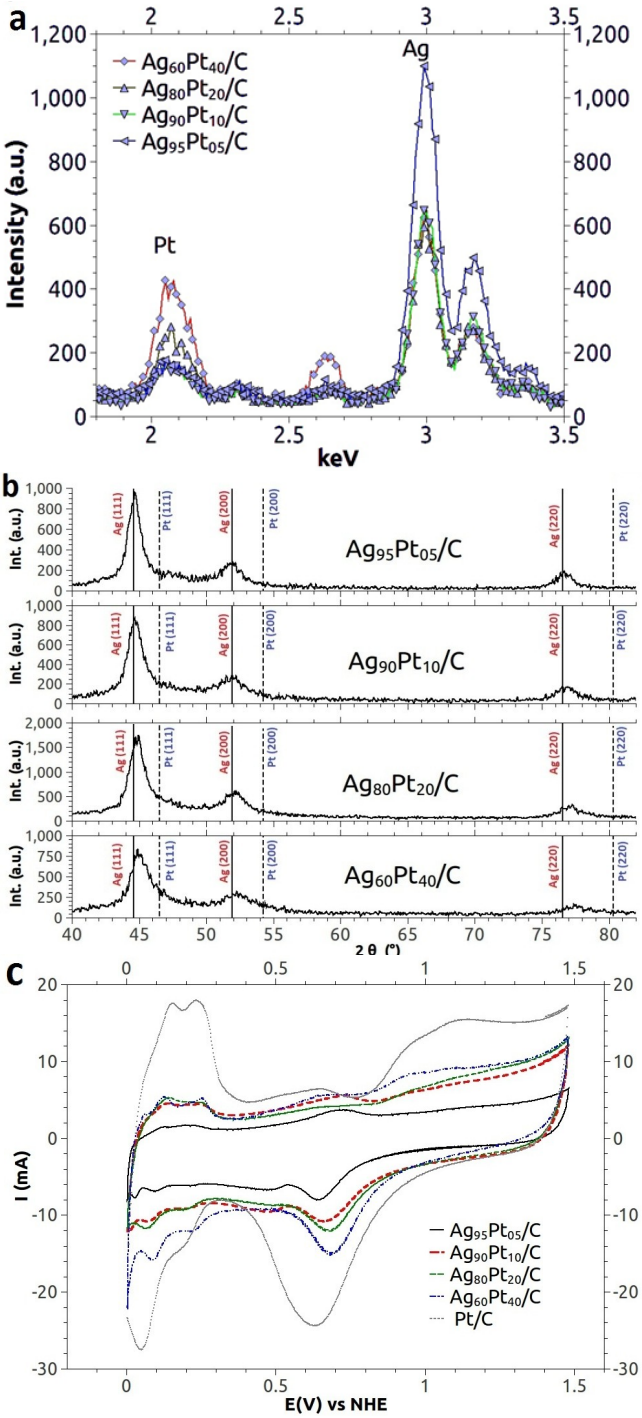

Figure 4. (a) Energy dispersive X-ray spectrometry and (b) X-ray diffraction for the samples whose compositions were confirmed to be $Ag_{95}Pt_{05}$/C, $Ag_{90}Pt_{10}$/C, $Ag_{80}Pt_{20}$/C and $Ag_{60}Pt_{40}$/C (c) Cyclic voltammetry curves at a scan rate of 200mVs^{-1}, in 0.5M H_2SO_4 solution saturated with N_2.

loidal silver. The UV/Vis spectra of the Ag_xPt_{100-x} samples show one broad peak with an absorption decreasing in the 350-450 range where the maximum absorption for silver is found, this change is

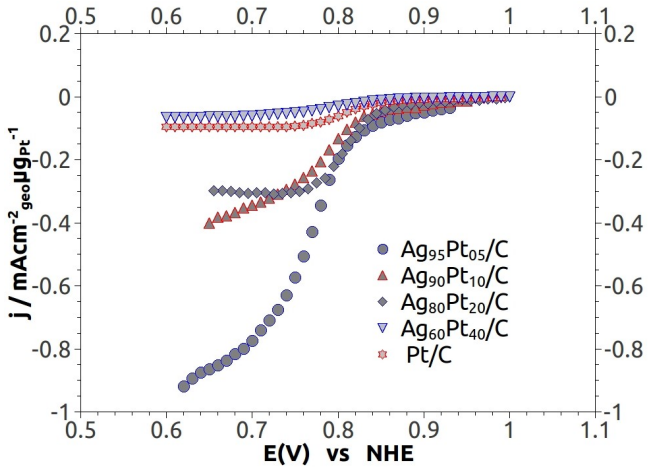

Figure 5. Steady-state current-potential curves for the electrocatalysts: $Ag_{95}Pt_{05}$/C, $Ag_{90}Pt_{10}$/C, $Ag_{80}Pt_{20}$/C and Pt/C, at different rotation rates, in an oxygen-saturated 0.5 M H_2SO_4 electrolyte, at 600 rpm.

attributed to the insertion of Pt atoms into the crystal lattice of Ag which modifies the plasmon properties [11].

Once the particles of each sample were supported on carbon, the morphology was studied using HR-TEM. The resulting images are shown in Fig. 3. The edge portion of each particle was darker than the central zone, which was a consequence of a higher density of atoms. This confirms the aim of the experimental work, in which it was sought that Pt atoms join on the surface of silver nanoparticles that form the core. The upper-left side of each image shows the diffraction pattern taken from the darker region of the particle; the patterns indicate a crystalline arrangement of atoms. The size distribution diagrams using samples of 50 particles had the highest frequency in the range of 6 -18 nm.

According to a semi-quantitative analysis by energy dispersive X-ray spectroscopy (Fig. 4a) the samples composition was approximately: $Ag_{95}Pt_{05}$/C, $Ag_{90}Pt_{10}$/C, $Ag_{80}Pt_{20}$/C and $Ag_{60}Pt_{40}$/C.

Characterization of the samples by X-ray diffraction (Fig. 4b) showed a slight displacement of the characteristic peaks of silver toward platinum positions, as the concentration of H_2PtCl_6 increased. The absence of the characteristic diffraction peaks of Pt in all the cases is a strong evidence of alloying between platinum and silver, as it has also been observed in other studies of core-shell systems [18, 19]. Accordingly, it is possible to argue that the core-shell morphology of the nanoparticles was modified as a function of the platinum precursor concentration. This is possible due to a galvanic substitution produced by the $[PtCl_6]^{2-}$ anion as has been reported by Zhao et al [11], according to the reaction:

$$4Ag + [PtCl_6]^{2-} \rightarrow Pt + 4Ag^{+} + 6Cl^{-} \quad (1)$$

According to Zhao et al., the $[PtCl_6]^{2-}$ anions attack uncovered silver nanoparticles and excavate the silver core of Ag@Pt nanoparticles, oxidizing Ag to Ag^+. The Ag^+ ions produced in the reaction are reduced again by trisodium citrate or $NaBH_4$ and the resultant Ag^0 atoms are alloyed with platinum atoms deposited on

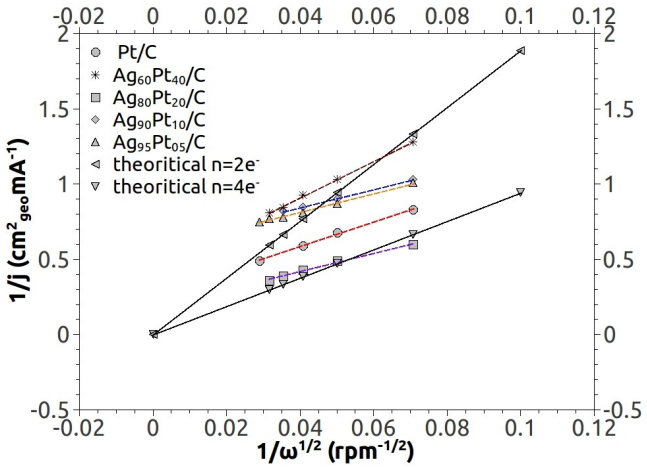

Figure 6. Koutecky-Levich (j^{-1} vs $\omega^{-1/2}$) plot at various electrode potentials, the density current values for all the samples were taken at E of 0.7 V.

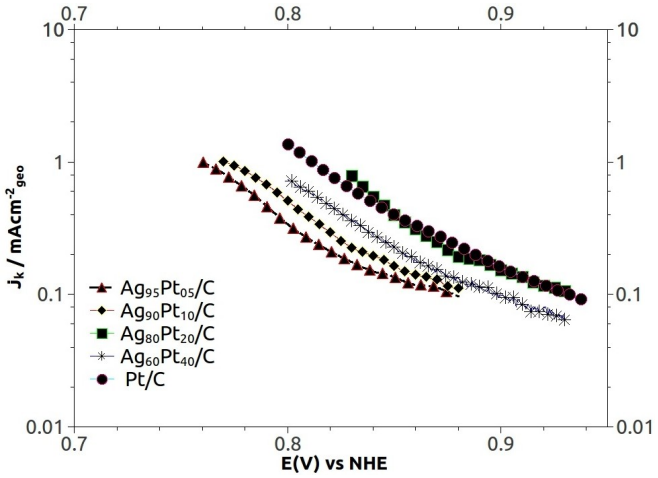

Figure 7. Mass transfer-corrected Tafel plots for the studied electrocatalysts in the region where the data fit was carried out.

the surface. This process produces ring-like nanostructures (Fig. 3). The same phenomenon has also been observed in Au-Ag systems when $HAuCl_4$ is used as precursor [10].

The XRD patterns only showed the presence of platinum as a displacement of the characteristic peaks of silver, but by cyclic voltammetry it was possible to distinguish its presence due to the high sensibility of this technique to elucidate electroactive metals located on catalytic surfaces (Fig. 4c). The electrochemical peaks associated to the adsorption and desorption of hydrogen (around 0.0-0.25V), the reduction of oxygen (around 0.65 V) and that of the onset of Pt oxide formation (around 0.80V) were a strong signal to elucidate the platinum presence. However small displacements of the positions of the peaks were observed that can be attributed to the effect of the incorporation of silver to Pt.

The electrochemical characterization of a catalyst deposited in a thin-layer rotating disk electrode in 0.5M H_2SO_4 solution led to the determination of the catalytic activity of the synthesized materials. From the analysis of the obtained curves (after charge transfer and mass transport correction), applying equations (2)-(4) (see below), the kinetic parameters of the ORR on the synthesized electrocatalysts were determined. Analysis results were important not only to get information about the ORR kinetics but also about the most probable pathway [20].

Due to the low solubility of oxygen in acidic media, the ORR depends strongly on the hydrodynamic conditions. The ORR characteristic set of polarization curves from TF-RDE measurements at 600 rpm is summarized in Fig. 5. Starting close to the open circuit potential (E_{oc}), and scanning the potential in cathodic direction, an increase of currents in the mixed kinetic-diffusion control region, in the range of -0.80 to -0.75 V/NHE for $Ag_{80}Pt_{20}$, $Ag_{60}Pt_{40}$ and Pt, and -0.76 to -0.70V/NHE for $Ag_{95}Pt_{05}$ and $Ag_{90}Pt_{10}$ was observed, followed by the appearance of a diffusion-limiting currents region. Carbon particles behavior shows an inferior activity in terms of larger overpotential, and smaller, almost negligible under the same electrode potential. High rotation rates accelerate oxygen to the electrode surface and result in large currents. The overall measured oxygen reduction reaction current density, (j), at several rotating speeds (ω), under different constant potentials, can be applied to construct Koutecky-Levich (K-L) plots, j^{-1} versus $\omega^{-1/2}$ (Fig. 6), based on the K-L equation:

$$\frac{1}{j}=\frac{1}{j_k}+\frac{1}{j_d}=\frac{1}{nFAkC_0}+\frac{1}{0.62nFAD_0^{2/3}\nu^{-1/6}C_0\omega^{1/2}} \quad (2)$$

Where j_k is the kinetic current density, j_d is the diffusion-limiting current density, n is the overall number of transferred electrons, F is the Faraday constant (96500 C mol^{-1}), k is the rate constant for oxygen reduction, C_0 is the saturated O_2 concentration in the electrolyte, D_0 is the diffusion coefficient of O_2, and ν is the kinetic viscosity of the solution. The number of electrons involved in the ORR is determined from the slope of the K-L curves. In this case ω is represented in rpm given by $\omega = 2\pi f/60$. The effect of the oxygen diffusion through the Nafion film is significant only when the electrode is covered with a thick film and can be neglected in the present study since the amount of Nafion in the prepared catalyst is sufficiently small. The experimental values obtained from Fig. 6 is in agreement with the theoretical value calculated for the four-electron transfer processes, using literature data for oxygen solubility, C_0 ($C_0 = 1.1 \times 10^{-6}$ mol cm^{-3}), oxygen diffusivity D ($D_0 = 1.4 \times 10^{-5} cm^2 s^{-1}$), and kinetic viscosity of the electrolyte, ν ($\nu = 1 \times 10^{-2} cm^2 s^{-1}$) [21].

Equation 2 allows to predict if the ORR follows the pathway of peroxide formation (n=2e$^-$) or a multielectron path (n=4e$^-$) for water formation, which is the case for the synthesized nanocatalysts of this research. From these results, we suggest that oxygen reduction may proceed via the overall four-electron transfer reaction to water formation, i.e., $O_2+4H^++4e^-\rightarrow 2H_2O$. This means that the pathway toward peroxide formation is less favorable than water formation.

The catalytic activity of the bimetallic nanomaterial can be measured in terms of the electrochemical kinetic parameters deduced from the mass transfer-corrected Tafel slopes [22]. Fig. 7 shows Tafel plot, using the data of Fig. 5, previously

corrected to give the kinetic current density, j_k determined using the equation:

$$j_k = \frac{j_d j}{j_d - j} \quad (3)$$

where j and j_d are the overall and diffusion-limiting current densities described above. The basis of the potential dependence of the electrochemical reaction rates, expressed as kinetic current density, is the Tafel equation, $\eta_k = a + b \log j$, where b is the so-called Tafel slope, conventionally written in the form of the following equation:

$$b = -\frac{d \log j_k}{dE} = -2.3\frac{RT}{n\alpha F} \quad (4)$$

where n and α are the number of electrons transferred and the charge transfer coefficient, respectively, and b is one of the most frequently used diagnostic criteria in the elucidation of the electrochemical reaction mechanism. It is well known that the rate of the ORR is directly related to the exchange current density, j_0, and exponentially related to b. Table 1 summarized the kinetic parameters deduced from the Tafel equation and reported for the same cathodic reaction on nanometric Ag_xPt_{100-x} and Pt, both obtained by our group of research in similar conditions and used for comparison. The Tafel parameters were in agreement with those reported for platinum in 0.5 M H_2SO_4 [23]. The exchange current density, j_0, was determined by extrapolation of the linear Tafel region to the reversible potential.

From an analysis of the exchange current density of Table 1 it can be seen that platinum is the material with the best catalytic activity, however the activity of the Ag_xPt_{10-x}/C catalysts is close to Pt/C despite the smaller mass of the platinum-containing catalysts. Even though there is not enough information to give a detailed explanation for certain changes in the electronic structure of platinum generated by the presence of silver as core, it is notorious that a small amount of platinum inside the Ag structure modifies the electrochemical behavior of Ag. Moreover, it can be observed that the studied materials had a Tafel slope, b, in or near the range of 0.060-0.120 V/dec, which is characteristic of the ORR mechanism where the rate determining step is the first electron transfer to oxygen adsorbed on the catalyst surface [24]. Results reveal that these materials could be considered as strong candidates to be used as cathodes for PEM fuel cells. The characterization of the membrane electrode assembles (MEA's) are in processing. Those results will be a strong indicator for determining if the material can be used in practical applications.

4. CONCLUSIONS

Ag_xPt_{100-x}/C colloidal nanostructured catalysts with activity for the ORR were prepared by sequential reduction of $AgNO_3$ and H_2PtCl_6, using an ultrasound-assisted colloidal method. Results of the physical characterization showed ring-like morphology with size distribution in the range of 6-16 nm for each sample. The singular morphology was attributed to the galvanic substitution produced by $[PtCl_6]^{2-}$ anions as it was reported by Zhao[11]. The ORR favored a multielectronic path (n=4e$^-$) for water formation with catalytic activity towards the ORR similar to polycrystalline platinum. This activity was inferred from the electrochemical kinetic parameters, which correspond to the exchange current density, charge transfer coefficient and Tafel slope. So these materials are good candidates to be used as cathodes for PEM fuel cells.

5. ACKNOWLEDGEMENTES

This work was partially supported by the National Science and Technology Council of Mexico (CONACYT, project 83247). Special thanks are due to Professor Miguel J. Yacaman, from the International Center for Nanotechnology and Advanced Materials (ICNAM), at the University of Texas - San Antonio, U.S.A., for assistance with HRTEM observations and to Luzma Avilés-Arellano for her technical support.

REFERENCES

[1] P.P. Edwards, V.L. Kuznetsov, W.I.F. David, N.P. Brandon, Energ Policy, 36, 4356 (2008).
[2] P. Corbo, F. Migliardini, O. Veneri, J Power Sources, 195, 7849 (2010).
[3] J. Brouwer, Curr Appl Phys., 10, S9 (2010).
[4] T. Okada, E. Yoo, T. Kahara, C. Ono, J. Nakamura, Electrochem Solid St., 11, B96 (2008).
[5] T. Ohsaka, M.R. Miah, J. Masud, Electrochim Acta, 56, 285 (2010).
[6] M.R. Miah, M.T. Alam, T. Okajima, T. Ohsaka, J. Electrochem Soc., 156, B1142 (2009).
[7] X.S. Zhang, J.S. Zheng, P. Li, J. Zhu, X.G. Zhou, W.K. Yuan, Electrochem Commun., 9, 895 (2007).
[8] K. Epping Martin, P. Kopasz John, W. McMurphy Kevin, Status of Fuel Cells and the Challenges Facing Fuel Cell Technology Today, in: Fuel Cell Chemistry and Operation, American Chemical Society, 2010, pp. 1-13.
[9] R.R. Adzic, K. Sasaki, H. Naohara, Y. Cai, Y.M. Choi, P. Liu, M.B. Vukmirovic, J.X. Wang, Angew Chem. Int. Edit., 49,

Table 1. Electrochemical kinetic parameters obtained by thin-film rotating disk electrode

Material	E_{OC} (V)	α	-b(V/dec)	j_0(mAcm$^{-2}_{geo}$)
$Ag_{95}Pt_{05}$/C	0.930± 0.005	0.53 ± 0.02	0.115 ± 0.002	7.0±0.4 × 10^{-5}
$Ag_{90}Pt_{10}$/C	0.950 ± 0.004	0.56 ± 0.03	0.107 ± 0.003	5.0±0.5 × 10^{-5}
$Ag_{80}Pt_{20}$/C	0.982 ± 0.006	0.54 ± 0.01	0.110 ± 0.005	1.8±0.2 × 10^{-4}
$Ag_{60}Pt_{40}$/C	0.983± 0.008	0.52 ± 0.02	0.116 ±0.003	1.5±0.3 × 10^{-4}
Pt/C	0.990 ± 0.007	0.53 ± 0.01	0.114 ± 0.004	2.3±0.2 × 10^{-4}

8602 (2010).
[10]Y. Sun, B. Mayers, Y. Xia, Advanced Materials, 15, 641 (2003).
[11]D. Zhao, Y.-H. Wang, B. Yan, B.-Q. Xu, J. Phys. Chem. C, 113, 1242 (2009).
[12]L. Chen, W. Zhao, W. Jiao, X. He, J. Wang, Y. Zhang, Spectrochim. Acta A, 68, 484 (2007).
[13]P.V. Kamat, Z.S. Pillai, J. Phys. Chem. B, 108, 945 (2004).
[14]B.Q. Xu, D. Zhao, Y.H. Wang, B. Yan, J. Phys. Chem. C, 113, 1242 (2009).
[15]B.G. Ershov, Russ Chem B+, 50, 626 (2001).
[16]E. Antolini, Appl. Catal. B-Environ, 88, 1 (2009).
[17]A. Gedanken, Ultrason Sonochem., 11, 47 (2004).
[18]M. Mavrikakis, S. Alayoglu, A.U. Nilekar, B. Eichhorn, Nat. Mater., 7, 333 (2008).
[19]B. Eichhorn, S. Alayoglu, P. Zavalij, Q. Wang, A.I. Frenkel, P. Chupas, Acs. Nano, 3, 3127 (2009).
[20]O. Solorza-Feria, G. Ramos-Sanchez, Int. J. Hydrogen Energy, 35, 12105 (2010).
[21]C. Contanceu, P. Crouigneau, J.P. Léager, C. Lamy, J. Electro-anal. Chem., 379, 389 (1994).
[22]R.G. Gonzalez-Huerta, A.R. Pierna, O. Solorza-Feria, J. New Mat. Electrochem. Systems, 11, 63 (2008).
[23]U.A. Paulus, T.J. Schmidt, H.A. Gasteiger, R.J. Behm, J. Electroanal. Chem., 495, 134 (2001).
[24]U.A. Paulus, A. Wokaun, G.G. Scherer, T.J. Schmidt, S.V.R. V, N.M. Markovic, P.N. Ross, J. Phys. Chem. B, 106, 4181 (2002).